JOURNAL OF PHYSICAL ORGANIC CHEMISTRY
J. Phys. Org. Chem. 2007; **17:** 1007–1016
Published online 13 August 2004 in Wiley InterScience (www.interscience.wiley.com). DOI: 10.1002/poc.820

Kinetics and thermodynamics of C—Cl bond activation by $[Ir(CO)_2Cl_2]^-$†

Paul W. Vickers, Jean M. Pearson, Talit Ghaffar, Harry Adams and Anthony Haynes*

Department of Chemistry, University of Sheffield, Sheffield S3 7HF, UK

Received 25 August 2003; revised 1 March 2004; accepted 10 March 2004

epoc ABSTRACT: Kinetic measurements are reported for the oxidative addition reactions of methyl chloride and acetyl chloride with $[Ir(CO)_2Cl_2]^-$. At 40 °C the second-order rate constant for MeCOCl addition is estimated to be nearly 40 000 times larger than that for MeCl addition. The Ir(III) products, $[Ir(CO)_2Cl_3R]^-$ (R = Me, COMe) have been isolated and characterised by spectroscopy and x-ray crystallography. In the absence of excess organic chloride, both Ir(III) complexes undergo reductive elimination of RCl. Kinetic measurements show these reactions to be first order in the Ir(III) complex with elimination of MeCOCl estimated to be ca 7000 times faster than MeCl elimination at 40 °C. Combination of activation parameters for the forward and reverse reactions allows calculation of thermodynamic parameters for oxidative addition. Both MeCl and MeCOCl additions are exothermic (by 44 and 68 kJ mol^{-1}, respectively) but disfavoured entropically. The trends are predicted satisfactorily by *ab initio* and DFT computational methods. The results for MeCl addition to $[Ir(CO)_2Cl_2]^-$ are compared with data for MeI addition to $[Ir(CO)_2I_2]^-$. Kinetic data are also reported for carbonylation of $[Ir(CO)_2Cl_3Me]^-$ into $[Ir(CO)_2Cl_3(COMe)]^-$ under mild conditions in PhCl–MeOH. It is concluded that the low activity of iridium–chloride carbonylation catalysts is due primarily to the relatively slow reaction of $[Ir(CO)_2Cl_2]^-$ with MeCl. Copyright © 2004 John Wiley & Sons, Ltd.
Additional material for this paper is available in Wiley Interscience

KEYWORDS: iridium; carbonyl; halide; oxidative addition; kinetics; thermodynamics

INTRODUCTION

Activation of organic molecules by oxidative addition to transition metal complexes plays a key role in many catalytic processes.[1] In a typical oxidative addition reaction, cleavage of a covalent bond in the substrate is accompanied by formation of two new metal—ligand bonds to give a product complex in which the coordination number and formal oxidation state of the transition metal are both raised by two, Eqn (1). The reverse of this process, reductive elimination, is often the step in a catalytic cycle by which an organic product is released from the transition metal centre.

$$[L_nM] + X - Y \rightleftharpoons [L_nM(X)(Y)] \qquad (1)$$

Many of the fundamental studies of oxidative addition reactions have been carried out using Vaska's complex, *trans*-$[Ir(CO)(PPh_3)_2Cl]$ and its analogues.[2] Such square planar d^8 Ir(I) complexes react with a variety of substrates, including H_2, HX, X_2 and RX (X = halide, R = alkyl, aryl or acyl). The kinetics and thermodynamics of oxidative addition depend on the steric and electronic properties of the coordinated ligands and on the substrate being added. Oxidative addition of methyl iodide and reductive elimination of acetyl iodide are key steps in the industrial processes for carbonylation of methanol to acetic acid, catalysed by $[M(CO)_2I_2]^-$ (M = Rh, Ir).[3,4] Although methyl iodide is found to be the most effective co-catalyst in these processes, methyl chloride has also been used in some studies. For example, Gelin *et al*. found that MeCl is almost as effective as MeI as a promoter for the vapour phase carbonylation of methanol, using Ir dicarbonyl species entrapped in zeolite cavities.[5]

In this paper we report the reactivity of $[Ir(CO_2Cl_2]^-$ with methyl chloride and acetyl chloride. In each case, the kinetics of both the forward (oxidative addition) and reverse (reductive elimination) reaction have been measured, enabling thermodynamic parameters to be estimated and compared with the results of theoretical calculations. X-ray crystal structures of the Ir(III) products are reported, as well as kinetic data for carbonylation of $[Ir(CO)_2Cl_3Me]^-$ into $[Ir(CO)_2Cl_3(COMe)]^-$. Implications for halide effects on methanol carbonylation activity are considered.

**Correspondence to:* A. Haynes, Department of Chemistry, University of Sheffield, Sheffield S3 7HF, UK.
E-mail: a.haynes@sheffield.ac.uk
†Paper presented at the 9th European Symposium on Organic Reactivity, 12–17 July 2003, Oslo, Norway.
Contract/grant sponsor: BP Chemicals Ltd and EPSRC.

RESULTS AND DISCUSSION

Oxidative addition of MeCl to $[Ir(CO)_2Cl_2]^-$

The tetraphenylarsonium salt of $[Ir(CO)_2Cl_2]^-$ was found to react very slowly with neat MeCl at 55 °C. After several days, a pure sample of $Ph_4As[Ir(CO)_2Cl_3Me]$ was isolated and characterised by IR and NMR spectroscopy and by elemental analysis. In the IR spectrum, two strong ν(CO) absorptions at 2116 and 2056 cm^{-1} are consistent with a *cis*-dicarbonyl geometry for $[Ir(CO)_2Cl_3Me]^-$. The methyl ligand gives rise to resonances at δ 1.6 and δ −13.7, respectively, in the ^1H and ^{13}C NMR spectra, while the two equivalent CO ligands give a ^{13}C resonance at δ 156.1. The *fac–cis* geometry of $[Ir(CO)_2Cl_3Me]^-$ was confirmed by an x-ray crystal structure of $Ph_4As[Ir(CO)_2Cl_3Me]$ (*vide infra*).

The kinetics of the reaction of $[Ir(CO)_2Cl_2]^-$ with MeCl were monitored using IR spectroscopy. Since MeCl exists as a gas at room temperature and pressure, experiments were performed by condensing MeCl into a Fisher Porter vessel at −196 °C. The sealed vessel was then warmed to the required temperature (40–55 °C), generating a vapour pressure of 7–10 atm. At regular time intervals the pressure was released allowing the MeCl to evaporate, hence quenching the reaction. The resulting mixture of solid $[Ir(CO)_2Cl_2]^-$ and $[Ir(CO)_2Cl_3Me]^-$ was dissolved in CH_2Cl_2 and an IR spectrum recorded. During the reaction, the two ν(CO) bands of $[Ir(CO)_2Cl_2]^-$ at 2054 and 1971 cm^{-1} decayed and new absorptions due to $[Ir(CO)_2Cl_3Me]^-$ grew at 2116 and 2056 cm^{-1}. The intensities of the well resolved reactant and product bands at 1971 and 2116 cm^{-1}, respectively, were used to generate concentration vs time plots for the two Ir species. The decay in concentration of $[Ir(CO)_2Cl_2]^-$ was well fitted by an exponential curve, showing the reaction to be first order in the Ir(I) complex. Values of the observed pseudo-first-order rate constant, k_{obs}, are given in Table 1.

Since neat MeCl was employed as both reactant and solvent to achieve convenient reaction rates, it was not feasible to determine the order of the reaction in MeCl by measuring the dependence of k_{obs} on [MeCl]. If it is assumed that the reaction is first order in MeCl (and therefore second order overall) as commonly found for this type of reaction,[2,6–8] the second-order rate constant, k_1, can be calculated using $k_1 = k_{obs}/[MeCl]$ (with [MeCl] = 18.14 M for neat methyl chloride). Values of k_1 over the range 40–55 °C are given in Table 1 and activation parameters calculated from the slope and intercept of an Eyring plot [$\ln(k_1/T)$ vs $1/T$] are given in Table 5. The large negative entropy of activation is consistent with the reaction proceeding through a highly ordered transition state, typical of an S_N2-type reaction mechanism (Scheme 1).[9]

Table 1. Kinetic data for MeCl addition to $[Ir(CO)_2Cl_2]^-$ (in neat MeCl)

T(°C)	$10^6 k_{obs}$ (s^{-1})	$10^7 k_1$ ($M^{-1} s^{-1}$)
40	2.56	1.41
45	3.44	1.90
50	5.23	2.88
55	8.21	4.53

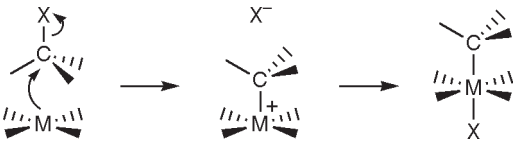

Scheme 1. S_N2 mechanism for oxidative addition of MeX to a square planar complex

Oxidative addition of MeCl to $[Ir(CO)_2Cl_2]^-$ is much slower than the analogous reaction of MeI with $[Ir(CO)_2I_2]^-$, for which kinetic data have been reported previously.[8] For example, at 40 °C we estimate that MeCl addition is ca 70 000 times slower than MeI addition. Although the most likely reason for the large difference in rates is the change in the alkyl halide substrate, the change in the halide ligands coordinated to Ir may also contribute. We therefore measured the kinetics of oxidative addition of MeI to $[Ir(CO)_2Cl_2]^-$ for comparison. The reaction of $[Ir(CO)_2Cl_2]^-$ with MeI gives a mixture of two *cis*-dicarbonyl isomers of $[Ir(CO)_2Cl_2IMe]^-$, with the methyl ligand *trans* to either I or Cl. Full details of these experiments will be reported elsewhere. The second-order rate constant obtained (3.22×10^{-3} $M^{-1} s^{-1}$ at 25 °C in CH_2Cl_2) is very similar to that for the reaction of MeI with $[Ir(CO)_2I_2]^-$ (3.09×10^{-3} $M^{-1} s^{-1}$). Therefore the much lower reactivity observed for the MeCl reaction is clearly due to the nature of the alkyl halide. Qualitative tests on the reaction of MeBr with $[Ir(CO)_2Br_2]^-$ revealed a reactivity intermediate between the chloride and iodide systems. The reaction was found to reach completion in within 48 h using 2 M MeBr in *t*-BuOMe at 75 °C.

Our results concur with the trend in reactivity found for alkyl and aryl halides in other oxidative addition reactions. For example, the rate of reaction of *trans*-$[Ir(PPh_3)_2(CO)Cl]$ with methyl halides[6] and with *p*-tolyl halides.[10] decreases in the order RI > RBr > RCl. Collman and Maclaury reported that oxidative addition to a rhodium(I) macrocycle complex is more than 10^5 times faster for $C_5H_{11}I$ than for $C_5H_{11}Cl$.[11] This trend reflects the increase in C—X bond dissociation energy [D(C—X)/kJ mol^{-1} 327, X = Cl; 285, X = Br; 213, X = I).[12] The results of both experimental[2,6,13] and theoretical[9,14] studies indicate that oxidative addition of methyl halides to square planar d^8 complexes proceeds via initial nucleophilic attack by the metal centre on the methyl carbon (Scheme 1). The S_N2 type transition state will have a significantly weakened C—X bond, and hence the activation barrier is expected to be sensitive to the reactant C—X bond strength.

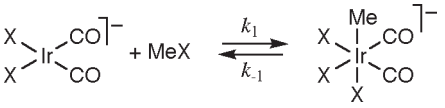

Scheme 2. Oxidative addition of MeX to $[Ir(CO)_2X_2]^-$ (X = Cl, I)

Reductive elimination of MeCl from $[Ir(CO)_2Cl_3Me]^-$

The stability of $[Ir(CO)_2Cl_3Me]^-$ at elevated temperatures was studied using *in situ* high pressure IR spectroscopy. When a solution of $Bu_4N[Ir(CO)_2Cl_3Me]$ in chlorobenzene was heated above 90 °C under N_2 (5 atm), the two ν(CO) bands of $[Ir(CO)_2Cl_3Me]^-$ at 2111 and 2052 cm^{-1} were replaced by bands due to $[Ir(CO)_2Cl_2]^-$ at 2051 and 1970 cm^{-1}, indicating reductive elimination of MeCl from the Ir(III) methyl complex (Scheme 2). The decay of $[Ir(CO)_2Cl_3Me]^-$ was found to obey first-order kinetics, and values of the rate constant, k_{-1} are reported in Table 2. Activation parameters obtained from an Eyring plot of these data are given in Table 5. Combination of the activation parameters for oxidative addition and reductive elimination of MeCl allow the reaction thermodynamics to be estimated as ΔH^o −37 kJ mol^{-1} and ΔS^o −95 J mol^{-1} K^{-1}. Thus the oxidative addition reaction is exothermic, but disfavoured entropically.

Reductive elimination of MeI from $[Ir(CO)_2I_3Me]^-$

For comparison, we have conducted a study of reductive elimination of MeI from $[Ir(CO)_2I_3Me]^-$. On heating a solution of $Ph_4As[Ir(CO)_2I_3Me]$ in PhCl under N_2 to 100 °C, a weak absorption appeared in the IR spectrum at 1968 cm^{-1}, corresponding to the low frequency ν(CO) band of $[Ir(CO)_2I_2]^-$. This band reached a maximum intensity that remained constant for several hours, indicating an equilibrium lying in favour of the Ir(III)–methyl complex (Scheme 2, X = I).

In order to determine the kinetics of reductive elimination from $[Ir(CO)_2I_3Me]^-$, we monitored the rate of methyl exchange between $[Ir(CO)_2I_3CD_3]^-$ and CH_3I. The CD_3 labelled Ir complex displays weak IR bands at 2120 and 2065 cm^{-1} in addition to the strong ν(CO) bands at 2095 and 2045 cm^{-1}. The weaker pair of bands are assigned to ν(CD) vibrational modes, and on heating in the presence of excess CH_3I, these absorptions disappear [the ν(CO) bands remaining constant], due to the exchange reaction, Eqn (2).

$$[Ir(CO)_2I_3CD_3]^- + CH_3I\,(xs) \rightarrow [Ir(CO)_2I_3CH_3]^- + CD_3I \quad (2)$$

The kinetics of this reaction were found to be first order in $[Ir(CO)_2I_3CD_3]^-$. Assuming that the methyl exchange occurs via a stepwise reductive elimination–oxidative addition sequence, the observed rate constant can be equated to k_{-1} for reductive elimination of CD_3I from $[Ir(CO)_2I_3CD_3]^-$. Values of k_{-1} are given in Table 2 and are ca 30 times larger than the corresponding rate constants for elimination of MeCl from $[Ir(CO)_2Cl_3Me]^-$. Activation parameters derived from an Eyring plot of the data are given in Table 5. Combination of these parameters with published data[8] for the oxidative addition of MeI to $[Ir(CO)_2I_2]^-$ allows estimation of thermodynamic parameters ΔH^o −44 kJ mol^{-1} and ΔS^o −56 J mol^{-1} K^{-1}. Thus the oxidative addition process is more exothermic for MeI than for MeCl.

Table 2. Kinetic data for MeX elimination from $[Ir(CO)_2X_3Me]^-$ (X = Cl, I) (in PhCl)

T(°C)	$10^6 k_{-1}$ (s^{-1}) X = Cl	$10^4 k_{-1}$ (s^{-1}) X = I
93	3.94	1.05
108	8.02	3.36
119	26.9	9.00
132	91.9	25.4

Oxidative addition of MeCOCl to $[Ir(CO)_2Cl_2]^-$

The reaction of acetyl chloride with $[Ir(CO)_2Cl_2]^-$ to give $[Ir(CO)_2Cl_3(COMe)]^-$ has been reported by Forster.[15] We have used a similar procedure to isolate $Ph_4As[Ir(CO)_2Cl_3(COMe)]$, which was characterised by IR and NMR spectroscopy and elemental analysis. Spectroscopic data are given under Experimental and are consistent with a *fac–cis* geometry for $[Ir(CO)_2Cl_3(COMe)]^-$, analogous to $[Ir(CO)_2Cl_3Me]^-$. This structure was confirmed by an x-ray crystal structure (*vide infra*).

The kinetics of oxidative addition of acetyl chloride to $[Ir(CO)_2Cl_2]^-$ were monitored by IR spectroscopy using acetonitrile as the solvent. The concentration of acetyl chloride was kept in large excess over [Ir] in order to achieve pseudo-first-order conditions. The kinetic data for each experiment were well fitted by an exponential curve, showing the reaction to be first order in $[Ir(CO)_2Cl_2]^-$. Observed pseudo-first-order rate constants, k_{obs}, are given in Table 3. A plot of k_{obs} vs [MeCOCl] at constant temperature (25 °C) is linear, indicating the reaction to be first order in MeCOCl and therefore second order overall. The second-order rate constant, k_2, obtained from the gradient of this plot is 2.09 ($\pm$0.1) × 10^{-3} M^{-1} s^{-1}. Kinetic measurements were also made over the temperature range 5–35 °C and second-order rate constants were calculated using $k_2 = k_{obs}$/[MeCOCl], assuming that second-order behaviour persists at each temperature. Activation parameters

Table 3. Kinetic data for MeCOCl addition to $[Ir(CO)_2Cl_2]^-$ (in MeCN)

	$10^4 k_{obs}(s^{-1})$					
T(°C)	0.1 M MeCOCl	0.2 M MeCOCl	0.3 M MeCOCl	0.4 M MeCOCl	0.5 M MeCOCl	$10^3 k_2(M^{-1} s^{-1})$
5	0.755					0.755
15	1.63					1.63
25	2.11	4.63	6.64	8.12	10.8	2.09
34	4.18					4.18

calculated from an Eyring plot of the data are given in Table 5, the large negative value of $\Delta S^{\ddagger}$ being consistent with an associative mechanism. Extrapolation to 40 °C predicts a rate constant for the addition of MeCOCl to $[Ir(CO)_2Cl_2]^-$ of $5.3 \times 10^{-3}\,M^{-1}\,s^{-1}$, which is nearly 40 000 times larger than that for MeCl addition at the same temperature. This difference in rate constant arises from a lowering of $\Delta H^{\ddagger}$ by 27 kJ mol^{-1}.

Reductive elimination of MeCOCl from $[Ir(CO)_2Cl_3(COMe)]^-$

This reaction has been described briefly by Forster,[16] and occurs under much milder conditions (25–60 °C) than elimination of methyl chloride from $[Ir(CO)_2Cl_3Me]^-$ (90–130 °C). When a solution of $Bu_4N[Ir(CO)_2Cl_3(COMe)]$ in MeCN was monitored by IR spectroscopy, conversion of the acetyl complex into $[Ir(CO)_2Cl_2]^-$ and MeCOCl was observed, until an equilibrium was attained in which a significant amount of the acetyl complex remained (Scheme 3).

In order to drive the reductive elimination to completion, an amine was added to scavenge the acetyl chloride. In the presence of excess diphenylamine, IR spectroscopy indicated the conversion of $[Ir(CO)_2Cl_3(COMe)]^-$ (2128, 2074, 1690, 1670 cm^{-1}) into $[Ir(CO)_2Cl_2]^-$ (2054, 1971 cm^{-1}). In addition, an absorption grew at 1666 cm^{-1}, corresponding to the amide, Ph_2NCOMe (confirmed by a separate reaction of acetyl chloride with diphenylamine in MeCN). The reaction stoichiometry can be defined as Eqn (3), the HCl produced presumably being scavenged by the amine to give $[Ph_2NH_2]Cl$.

$$[Ir(CO)_2Cl_3(COMe)]^- + Ph_2NH \rightarrow [Ir(CO)_2Cl_2]^- + Ph_2NCOMe + HCl \quad (3)$$

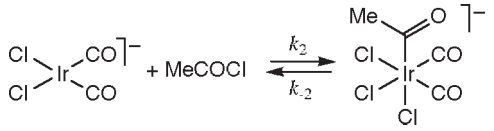

Scheme 3. Oxidative addition of MeCOCl to $[Ir(CO)_2Cl_2]^-$

Under these conditions the decay of $[Ir(CO)_2Cl_3(COMe)]^-$ goes to completion and follows simple pseudo-first-order kinetics. Essentially identical rate constants were obtained for a range of amine concentrations (Table 4), indicating zero-order dependence on Ph_2NH. This confirms that the amine acts merely as a scavenger for acetyl chloride, and is not directly involved in the rate-determining step. When the more nucleophilic *N*-methyl aniline was used in place of diphenylamine, a first-order dependence of k_{obs} on [PhMeNH] indicated an alternative pathway involving direct nucleophilic attack of amine on the acetyl acomplex. Full details of these results will be reported elsewhere. The measured k_{obs} values can therefore be equated with the rate constant for reductive elimination of acetyl chloride (k_{-2}). Some solvent dependence was observed, with a significantly slower rate being observed in the less polar chloroform. Activation parameters calculated from an Eyring plot of the variable temperature data obtained in MeCN are given in Table 5. Based upon these data, elimination of MeCOCl is estimated to be ca 7000 times faster than elimination of MeCl at 40 °C.

Combination of the activation parameters for oxidative addition of MeCOCl and its reverse generates thermodynamic parameters for the reaction, ΔH^{o} −68 kJ mol^{-1} and ΔS^{o} −180 J mol^{-1} K^{-1}. Thus, the reaction of $[Ir(CO)_2Cl_2]^-$ with acetyl chloride is significantly more

Table 4. Kinetic data for MeCOCl elimination from $[Ir(CO)_2Cl_3(COMe)]^-$ (in MeCN, unless stated otherwise, with Ph_2NH added as MeCOCl scavenger at stated concentration)

	$10^5 k_{-2}(s^{-1})$			
T(°C)	0.08 M Ph_2NH	0.2 M Ph_2NH	0.3 M Ph_2NH	0.4 M Ph_2NH
26	0.833			
34	2.83			2.98
43	8.89			9.19
51	30.9	28.7	28.8	29.4
51	4.75[a]			
51	20.5[b]			
51	23.1[c]			
62	80.6			

[a] In $CHCl_3$.
[b] In THF.
[c] In $MeNO_2$.

Table 5. Activation parameters (conditions as described in the text)

Reaction	$\Delta H^{\ddagger}$/kJ mol^{-1}	$\Delta S^{\ddagger}$/J mol^{-1} K^{-1}
$[Ir(CO)_2Cl_2]^- + MeCl \rightarrow [Ir(CO)_2Cl_3Me]^-$	64 (±5)	−172 (±16)
$[Ir(CO)_2Cl_3Me]^- \rightarrow [Ir(CO)_2Cl_2]^- + MeCl$	101 (±13)	−77 (±34)
$[Ir(CO)_2I_2]^- + MeI \rightarrow [Ir(CO)_2I_3Me]^-$ (ref. 8)	54 (±1)	−113 (±4)
$[Ir(CO)_2I_3Me]^- \rightarrow [Ir(CO)_2I_2]^- + MeI$	98 (±2)	−56 (±4)
$[Ir(CO)_2Cl_2]^- + MeCOCl \rightarrow [Ir(CO)_2Cl_3(COMe)]^-$	37 (±5)	−171 (±18)
$[Ir(CO)_2Cl_3(COMe)]^- \rightarrow [Ir(CO)_2Cl_2]^- + MeCOCl$	105 (±4)	9 (±14)
$[Ir(CO)_2Cl_3Me]^- + CO \rightarrow [Ir(CO)_2Cl_3(COMe)]^-$	52 (±2)	−136 (±4)

exothermic than its reaction with methyl chloride. Similarly, the reaction enthalpies for oxidative addition of MeI and MeCOI to $[Ir(CO)(PMe_3)_2Cl]$ have been reported as ca 117 and 125 kJ mol^{-1}, respectively.[17]

Although the C—Cl bond strengths of methyl and acetyl chlorides are similar, addition of MeCOCl to $[Ir(CO)_2Cl_2]^-$ is more favourable, both thermodynamically and kinetically, than addition of MeCl. The C—Cl bond dissociation enthalpy of MeCOCl is calculated to be 354.1 kJ mol^{-1} based on standard enthalpies of formation for MeCOCl and the MeCO and Cl radicals. The stability of the Ir(III)–acetyl product may be enhanced by the π-acceptor nature of the acetyl ligand, whereas methyl is essentially a pure σ-donor. The difference in reactivity reflects the higher electrophilicity of acetyl chloride. Our data do not distinguish between ionic (S_N2) and concerted mechanisms for oxidative addition of MeCOCl. Recent DFT calculations identified a number of transitions states for concerted elimination of *cis*-acetyl and-iodide ligands from the analogous iodide, $[Ir(CO)_2(COMe)I_3]^-$ (and, by microscopic reversibility, for oxidative addition to $[Ir(CO)_2I_2]^-$).[18] For the *fac–cis* isomer, acetyl iodide elimination was calculated to have an activation energy of ca 120 kJ mol^{-1} and to be endothermic by ca 35 kJ mol^{-1}. An alternative S_N2 mechanism (possibly involving a tetrahedral intermediate, with negative charge localised on the carbonyl oxygen) was not considered in that study but cannot be ruled out by the experimental data.

Theoretical calculations

Computational methods were also employed to estimate the energetics of these oxidative addition reactions. Reactant and product geometries were optimised using both *ab initio* (MP2) and DFT (B3LYP) methods. The calculated reaction energies are summarised in Table 6 and compared with experimental values of reaction enthalpy, where available. The B3LYP results are in reasonable agreement with experiment, and concur that oxidative addition to $[Ir(CO)_2Cl_2]^-$ is more exothermic for MeCOCl than for MeCl. The MP2 results tend to overestimate the exothermicity of oxidative addition in all cases, but reproduce the experimentally observed trends, with oxidative addition being more exothermic for MeCOCl and MeI than for MeCl.

X-ray crystal structures

Crystallographic studies were carried out on the Ir(III) compounds, $Ph_4As[Ir(CO)_2Cl_3Me]$ and $Ph_4As[Ir(CO)_2Cl_3(COMe)]$. CCDC 217786 and 217787 contain supplementary crystallographic data for this paper. Both adopt a monoclinic crystal system with the *P*1 space group, and the Ph_4As^+ cations have the expected approximate tetrahedral geometry. The methyl complex $[Ir(CO)_2Cl_3Me]^-$ has a distorted coordination octahedral geometry, as illustrated in Fig. 1, with a facial set of three chloride ligands and *cis*-carbonyls. The coordination geometry around Ir in $[Ir(CO)_2Cl_3Me]^-$ is very similar to that reported for the chloride bridged dimer, $[Ir(CO)_2Cl_2Me]_2$.[19] The acetyl complex $[Ir(CO)_2Cl_3(COMe)]^-$ (Fig. 2) also has a distorted octahedral geometry, with the plane of the acetyl ligand rotated 85° relative to the approximate mirror plane of the $Ir(CO)_2Cl_3$ fragment. The bond lengths and angles in both structures (listed in Table 7) lie within the expected ranges. The Ir—Cl distances *trans* to CO are very similar in both complexes (ca 2.37 Å) whereas those *trans* to methyl (2.50 Å) or acetyl (2.56 Å) are significantly longer. This can be attributed to the strong *trans* influences of methyl and acetyl, which also lead to

Table 6. Computed energetics for oxidative addition reactions. Reactants and products optimised at MP2 and B3LYP levels using the LANL2DZ basis set

Reaction	ΔE (MP2)	ΔE (B3LYP)	ΔH^{o} (expt)
$[Ir(CO)_2Cl_2]^- + MeCl \rightarrow [Ir(CO)_2Cl_3Me]^-$	−81.6	−35.1	−37
$[Ir(CO)_2I_2]^- + MeI \rightarrow [Ir(CO)_2I_3Me]^-$	−97.0	−35.4	−44
$[Ir(CO)_2Cl_2]^- + MeCOCl \rightarrow [Ir(CO)_2Cl_3(COMe)]^-$	−104.6	−55.9	−68
$[Ir(CO)_2I_2]^- + MeCOI \rightarrow [Ir(CO)_2I_3(COMe)]^-$	−131.2	−65.6	—

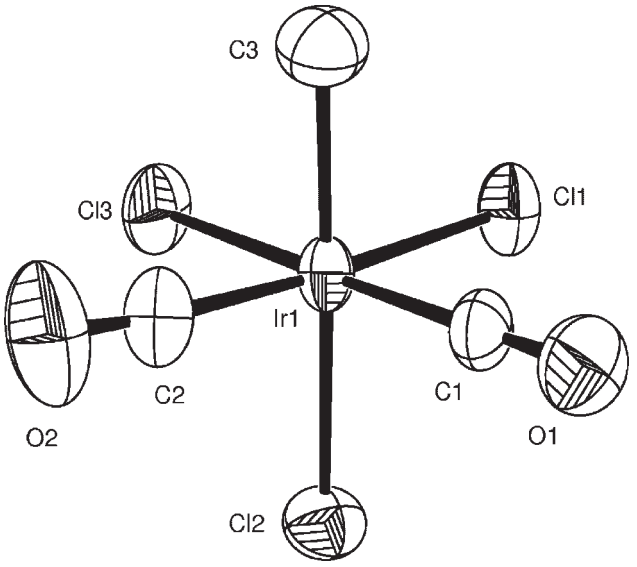

Figure 1. ORTEP plot of the $[Ir(CO)_2Cl_3Me]^-$ anion in the x-ray crystal structure of $Ph_4As[Ir(CO)_2Cl_3Me]$. Thermal ellipsoids are shown at the 50% probability level. Cation and hydrogen atoms are omitted for clarity

Table 7. Selected bond lengths (Å) and angles (°) from the x-ray crystal structures of $Ph_4As[Ir(CO)_2Cl_3Me]$ and $Ph_4As[Ir(CO)_2Cl_3(COMe)]$

	$[Ir(CO)_2Cl_3Me]^-$	$[Ir(CO)_2Cl_3(COMe)]^-$
Ir(1)—Cl(1)	2.386(2)	2.369(2)
Ir(1)—Cl(2)	2.500(2)	2.560(2)
Ir(1)—Cl(3)	2.365(2)	2.368(2)
Ir(1)—C(1)	1.875(9)	1.904(9)
Ir(1)—C(2)	1.873(10)	1.897(10)
Ir(1)—C(3)	2.114(10)	2.087(9)
C(1)—O(1)	1.094(10)	1.111(10)
C(2)—O(2)	1.114(12)	1.106(11)
C(3)—O(3)	—	1.186(11)
C(3)—C(4)	—	1.504(13)
O(1)—C(1)—Ir(1)	177.5(9)	177.9(8)
O(2)—C(2)—Ir(1)	175.0(11)	178.0(9)
C(2)—Ir(1)—C(1)	95.6(4)	96.4(4)
C(1)—Ir(1)—C(3)	92.3(4)	90.8(4)
C(2)—Ir(1)—C(3)	88.8(5)	92.4(4)
Cl(3)—Ir(1)—Cl(1)	91.35(9)	90.14(9)
C(3)—Ir(1)—Cl(1)	88.2(3)	88.2(3)
C(3)—Ir(1)—Cl(3)	87.5(3)	90.3(3)
C(3)—Ir(1)—Cl(2)	177.8(3)	179.1(3)
C(1)—Ir(1)—Cl(3)	178.7(3)	177.1(2)
C(2)—Ir(1)—Cl(1)	175.9(3)	176.3(3)
O(3)—C(3)—Ir(1)	—	120.0(7)
C(4)—C(3)—Ir(1)	—	119.0(7)

relatively low frequency ν(IrCl) absorptions for $[Ir(CO)_2Cl_3Me]^-$ (249 cm^{-1}) and $[Ir(CO)_2Cl_3$ (COMe)$]^-$ (229 cm^{-1}).

Carbonylation of $[Ir(CO)_2Cl_3Me]^-$

The organometallic reaction cycle for methanol carbonylation requires insertion of CO into a metal—methyl bond, in addition to the MeX oxidative addition and MeCOX reductive elimination steps discussed above. We have therefore investigated the reactivity of $[Ir(CO)_2Cl_3Me]^-$ with carbon monoxide, using *in situ* high-pressure IR spectroscopy. In PhCl at 93 °C, $[Ir(CO)_2Cl_3Me]^-$ was found to be unreactive towards CO (80 psi), whereas in a 1+1 v/v PhCl–MeOH solvent system, carbonylation of $[Ir(CO)_2Cl_3Me]^-$ (2119, 2060 cm^{-1}) into $[Ir(CO)_2Cl_3(COMe)]^-$ (2130, 2075, 1690 cm^{-1}) was achieved under relatively mild conditions (30–50 °C). The promotional effect of methanol has previously been noted for the iodide analogue, $[Ir(CO)_2I_3Me]^-$, and was explained by a mechanism involving substitution of I^- by CO, aided by a protic solvent.[20] Kinetic data obtained by monitoring the exponential decay of the band of $[Ir(CO)_2Cl_3Me]^-$ at 2119 cm^{-1} are listed in Table 8 and activation parameters are given in Table 5. An approximate first-order dependence on CO pressure is observed, consistent with a pre-equilbrium involving substitution of Cl^-. The activation parameters show a larger $\Delta H^{\ddagger}$ but a less negative $\Delta S^{\ddagger}$ for the chloride compared with the iodide. Under identical conditions (33 °C, 80 psi CO, 1:1 PhCl–MeOH) the observed pseudo-first-order rate constant for carbonylation of $[Ir(CO)_2Cl_3Me]^-$ is ca half that for $[Ir(CO)_2I_3Me]^-$. In these carbonylation experiments, the ν(CO) bands of $[Ir(CO)_2Cl_3(COMe)]^-$ reach a maximum before decaying (with $t_{1/2} \approx 20$ min at 33 °C) to give $[Ir(CO)_2Cl_2]^-$ (2059, 1978 cm^{-1}) and methyl acetate (1745 cm^{-1}). Thus, methanolysis of the iridium

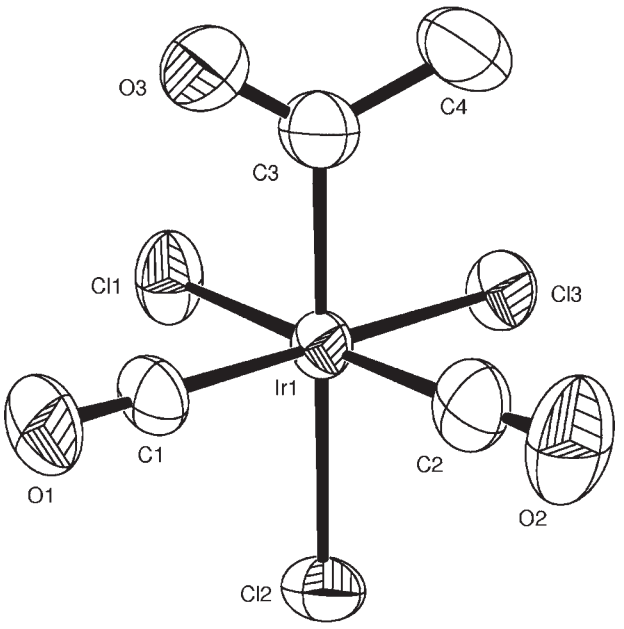

Figure 2. ORTEP plot of the $[Ir(CO)_2Cl_3(COMe)]^-$ anion in the x-ray crystal structure of $Ph_4As[Ir(CO)_2Cl_3(COMe)]$. Thermal ellipsoids are shown at the 50% probability level. Cation and hydrogen atoms are omitted for clarity

Table 8. Kinetic data for carbonylation of $[Ir(CO)_2Cl_3Me]^-$ (in 1:1 PhCl/MeOH)

CO pressure(psig)	T(°C)	$10^4 k_{obs}$ (s^{-1})
80	30	5.48
80	33	7.04
80	39	10.7
80	44	15.2
80	47	17.1
80	52	24.3
150	33	9.87
200	33	9.73
250	33	13.4
300	33	18.0
350	33	19.2
400	33	21.5

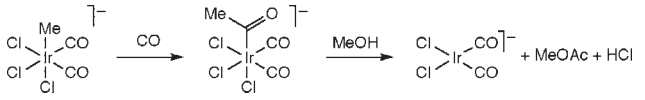

Scheme 4. Carbonylation of $[Ir(CO)_2Cl_3Me]^-$ in PhCl–MeOH

acetyl complex is also fairly facile under mild conditions (Scheme 4).

CONCLUSIONS

Kinetic measurements have been made for the oxidative addition of both MeCl and MeCOCl to $[Ir(CO)_2Cl_2]^-$. In each case the kinetics have also been measured for the reverse process, reductive elimination of RCl from $[Ir(CO)_2Cl_3R]^-$ (R = Me, COMe). Combination of activation parameters for the forward and reverse steps has allowed thermodynamic parameters to be estimated for the oxidative addition reactions. Addition of acetyl chloride has a lower activation barrier and is more thermodynamically favourable than addition of methyl chloride. In the series of reactions of MeX with $[Ir(CO)_2X_2]^-$, reaction rate decreases in the order X = I > Br > Cl, as found in related systems. This trend can be ascribed mainly to the increase in C—X bond strength. Carbonylation of $[Ir(CO)_2Cl_3Me]^-$ into $[Ir(CO)_2Cl_3(COMe)]^-$ occurs under mild conditions in PhCl–MeOH, at a rate comparable to that with the iodide analogue. Methanolysis of the Ir—acetyl species leads to formation of methyl acetate and $[Ir(CO)_2Cl_2]^-$. Using the experimental activation parameters in Table 5, extrapolated rate constants at 180 °C indicate that MeCl oxidative addition (at 1 M MeCl) would be ca 10^3–10^5 times slower than migratory CO insertion and MeCOCl reductive elimination. The lower catalytic activity of iridium–chloride compared with iridium–iodide based methanol carbonylation catalysts can therefore be ascribed to the much lower reactivity of Ir(I) with MeCl relative to MeI.

EXPERIMENTAL

Materials

All solvents used for synthesis or kinetic experiments were distilled and degassed prior to use following literature procedures.[21] Synthetic procedures were carried out utilizing standard Schlenk techniques. Nitrogen and carbon monoxide were dried through a short (20 × 3 cm diameter) column of molecular sieves (4 Å), which was regenerated regularly. Carbon monoxide was also passed through a short column of activated charcoal to remove any iron pentacarbonyl impurity.[22] The Ir complexes $[Ir(COD)Cl]_2$,[23] $Ph_4As[Ir(CO)_2I_2]$,[8] $Ph_4As[Ir(CO)_2Br_2]$[24] and $Ph_4As[Ir(CO)_2I_3Me]$[8] were synthesized according to literature procedures. Methyl iodide (Aldrich) was distilled over calcium hydride and stored in a foil-wrapped Schlenk tube under nitrogen and over mercury to prevent formation of I_2. Acetyl chloride, methyl chloride, methyl bromide, Ph_4AsCl (Aldrich) and $IrCl_3{\cdot}xH_2O$ (Johnson Matthey) were used as supplied.

Instrumentation

Ambient pressure FTIR solution spectra were measured using a CaF_2 liquid cell (0.1 or 0.5 mm path length) and either a PerkinElmer 1600 spectrometer or a Mattson Genesis spectrometer controlled by WINFIRST software. For ν(IrCl) absorptions below 400 cm^{-1}, IR spectra of nujol mulls between polyethylene sheets were recorded using a PerkinElmer 684 dispersive spectrometer. *In situ* high-pressure FTIR spectra were recorded using a Spectra-Tech Cylindrical Internal Reflectance (CIR) cell[25] and a PerkinElmer 1710 spectrometer fitted with an MCT detector. ^1H and ^{13}C NMR spectra were recorded using a Bruker WH400 or a Bruker AC250 spectrometer fitted with a Bruker B-ACS60 automatic sample changer operating in pulsed Fourier Transform mode, using the solvent as reference. Elemental analyses were performed using a PerkinElmer 2400 Elemental Analyzer.

Synthesis of Ir complexes

(a) $Ph_4As[Ir(CO)_2Cl_2]$. Ph_4AsCl (1.08 g, 2.6 mmol) was added to a solution of $[Ir(COD)Cl]_2$ (0.874 g, 1.3 mmol) in dichloromethane (25 cm^3) and stirred under an atmosphere of CO (2 h). The volume of the yellow solution was reduced and diethyl ether was added to crystallise the product. The pale yellow crystals were filtered and dried *in vacuo*; yield 1.243 g (68%). IR [CH_2Cl_2; ν(CO)/cm^{-1}]: 2054, 1971; [nujol; ν(IrCl)/cm^{-1}]: 329, 299. The Bu_4N^+ salt was prepared in an analogous manner using Bu_4NCl in place of Ph_4AsCl.

(b) $Ph_4As[Ir(CO)_2Cl_3Me]$. $Ph_4As[Ir(CO)_2Cl_2]$ (0.2 g, 0.28 mmol) was placed in a Fisher Porter tube. Excess

methyl chloride was condensed into the tube (−196 °C) which was then sealed. After allowing the vessel to warm up to room temperature it was heated to 55 °C (resulting in a pressure of 10 atm) and stirred for 7 days. The pressure in the Fisher Porter tube was released and the methyl chloride allowed to evaporate in the fume hood. The resulting solid was recrystallised from dichloromethane–diethyl ether and dried *in vacuo* to give orange crystals; yield 0.152 g (71%). Anal. Calcd for $C_{27}H_{23}As\ \ Cl_3IrO_2$: C, 43.1; H, 3.1; Cl, 14.1. Found: C, 42.5; H, 3.0; Cl, 14.5. IR (CH_2Cl_2; ν(CO)/cm^{-1}): 2116, 2056; [nujol; ν(IrCl)/cm^{-1}]: 327, 298 249. ^{1}H NMR ($CDCl_3$; δ): 1.6 (s, 3H, IrCH_3), 7.6–7.9 (m, 20H, *Ph*$_4$As). ^{13}C {^{1}H} NMR ($CDCl_3$; δ): 156.1 (*C*O), 135.0, 133.2, 131.7 (*Ph*$_4$As, *C*—H), 120.4 (*Ph*$_4$As, *C*—As), −13.7 (Ir*C*H$_3$). A suitable crystal was selected for an x-ray diffraction study (*vide infra*). The Bu_4N^+ salt was prepared in an analogous manner from $Bu_4N[Ir(CO)_2Cl_2]$.

(c) $Ph_4As[Ir(CO)_2Cl_3(COMe)]$. A variation of the method described by Forster[15] was used. $Ph_4As[Ir(CO)_2Cl_2]$ (49 mg, 70 μmol) was dissolved in dichloromethane (5 cm^3) and acetyl chloride (1 cm^3, excess) was added. After 10 min a dark green precipitate appeared. This was removed by filtration and discarded. The remaining yellow solution was evaporated to dryness and the resulting solid recrystallised from dichloromethane–diethyl ether and dried *in vacuo* to give yellow crystals; yield 0.043 g (78%). Anal. Calcd for $C_{28}H_{23}AsCl_3IrO_3$: C, 43.1; H, 3.0; Cl, 13.6. Found C, 42.9; H, 2.8; Cl, 13.7. IR [CH_2Cl_2; ν(CO)/cm^{-1}]: 2128 s, 2074 s 1690 m 1667 m; [nujol; ν(IrCl)/cm^{-1}]: 332, 305 229. ^{1}H NMR ($CDCl_3$; δ): 2.6 (s, 3H, COCH_3), 7.6–7.9 (m, 20H, *Ph*$_4$As). ^{13}C {^{1}H} NMR ($CDCl_3$; δ): 196.7 (*C*OMe) 153.0 (*C*O), 135.0, 133.0, 131.5 (*Ph*$_4$As, *C*—H), 120.3 (*Ph*$_4$As, *C*—As), 42.2 (CO*C*H$_3$). A suitable crystal was selected for an x-ray diffraction study (*vide infra*). The Bu_4N^+ salt was prepared in an analogous manner from $Bu_4N[Ir(CO)_2Cl_2]$.

Kinetic experiments

(a) Reaction of $[Ir(CO)_2Cl_2]^-$ with MeCl. $[Ir(CO)_2Cl_2]Ph_4As$ (0.5 g, 0.71 mmol) and a magnetic stirrer were placed in a glass Fisher Porter tube and connected to a gas manifold. The tube was cooled to −196 °C (liquid N_2) to condense MeCl (ca 15 cm^3) admitted from a cylinder. After sealing the tube it was allowed to warm up to room temperature resulting in a pressure of ca 4 atm. The tube was then heated using an oil bath (thermostatted to 40–55 °C using an Heidolph EKT 3000 contact thermometer). At regular timed intervals, the tube was removed from the oil bath and the pressure was released, allowing the MeCl to evaporate in the fumehood. The solid residue was dissolved in dichloromethane and a small sample was removed for FTIR analysis. The tube was then reconnected to the manifold and the solvent removed *in vacuo*. MeCl was condensed as before and the reaction was allowed to continue. The $Ph_4As[Ir(CO)_2Cl_3Me]$ product was recovered at the end of the reaction for use in other experiments.

(b) Reaction of $[Ir(CO)_2Cl_2]^-$ with MeCOCl. The required amount of acetyl chloride was placed in a 10 cm^3 graduated flask which was then made up to the mark with MeCN and shaken. A portion of this solution was used to record a background spectrum. Another portion (1 cm^3) was added to the solid complex $Ph_4As[Ir(CO)_2Cl_2]$ (7 mg, 10 μmol) in a sample vial to give a reaction solution containing 10 mM [Ir]. A portion of the reaction solution was quickly transferred into an IR cell (0.5 mm pathlength, CaF_2 windows), which was maintained at constant temperature throughout the kinetic run by a thermosttated jacket. FTIR spectra were recorded at regular time intervals using a Mattson Genesis spectrometer under computer control.

(c) Elimination of MeCOCl from $[Ir(CO)_2Cl_3(COMe)]^-$. The required amount of Ph_2NH (MeCOCl scavenger) was placed in a 10 cm^3 graduated flask which was then made up to the mark with the required solvent and shaken. A portion was used to record a background spectrum. Another portion (1 cm^3) was added to the solid complex $Bu_4N[Ir(CO)_2Cl_3(COMe)]$ (6 mg, 10 μmol) in a sample vial to give a reaction solution containing 10 mM [Ir]. A portion of the reaction solution was transferred into a thermostatted IR cell and the kinetic experiment performed using the same procedure as in (c) above.

(d) Reactivity of $[Ir(CO)_2Cl_3Me]^-$. The reaction solution was prepared by dissolving $[Ir(CO)_2Cl_3Me]Bu_4N$ (0.18 g, 0.29 mmol) in PhCl (8 cm^3). The solution was filtered into the high-pressure IR cell and the head fitted. The cell was flushed at least four times with N_2 or CO, as required (whilst stirring the solution) and then pressurised with 5 atm N_2 or the required pressure of CO. The cell was then heated to the required temperature and FTIR spectra were recorded at regular time intervals under computer control.

(e) Data analysis. After each kinetic run, absorbance vs time data for the appropriate ν(CO) absorptions were extracted and analysed off-line using Kaleidagraph curve-fitting software. First-order (or pseudo-first-order) rate constants were obtained from fitting exponential curves to the experimental data (correlation coefficients $\geq$0.999). Each kinetic run was repeated at least twice to check reproducibility, the k_{obs} values given being averaged values with component measurements deviating from each other by $\leq$5%.

X-ray structure determinations. Three-dimensional, room temperature x-ray data were collected in the

Table 9. Summary of crystallographic data

Parameter	$Ph_4As[Ir(CO)_2Cl_3Me]$	$Ph_4As[Ir(CO)_2Cl_3(COMe)]$
Formula	$C_{27}H_{23}AsCl_3IrO_2$	$C_{28}H_{23}AsCl_3IrO_3$
Formula wt	752.92	780.93
Cryst syst.	triclinic	triclinic
Space group	$P\bar{1}$	$P\bar{1}$
Colour	pale yellow	yellow
a (Å)	9.331(3)	9.162(3)
b (Å)	12.173(3)	12.371(3)
c (Å)	13.578(3)	14.176(6)
α (°)	108.66(2)	109.01(3)
β (°)	107.59(3)	108.79(3)
γ (°)	92.68(2)	92.48(3)
Temp. (K)	293(2)	293(2)
Z	2	2
Final R indices [$I > 2\sigma(I)$]	$R1 = 0.0475$	$R1 = 0.0396$
	$wR_2 = 0.1188$	$wR_2 = 0.1011$
R indices (all data)	$R1 = 0.0561$	$R1 = 0.0435$
	$wR_2 = 0.1245$	$wR_2 = 0.1042$
GOF	1.043	1.022

range $3.5 < 2\theta < 45°$ on a Siemens P4 diffractometer by the omega scan method using Mo-K_α radiation ($\bar{\lambda} = 0.71073$ Å). The structures were solved by direct methods and refined by full matrix least squares on F^2. Hydrogen atoms were included in calculated positions and refined in riding mode. Complex scattering factors were taken from the program package SHELXL93[26] as implemented on the Viglen 486dx computer. Crystallographic data are summarized in Table 9 and full listings of data are given in the Supplementary Material.

Computational details

Quantum mechanical calculations using second-order Møller-Plesset (MP2) theory or DFT (B3LYP) were performed using the Gaussian94 suite of programs.[27] Geometries of reactant and product molecules were optimized using the Berny algorithm[28] as implemented in Gaussian94 and the LANL2DZ Gaussian basis set developed by Hay and Wadt.[29] This uses a semi-core double-ζ contraction scheme for the heavy elements Ir, and Cl, with the light atoms C, O and H being described by the split-valence Dunning 9-5V all-electron basis.

Acknowledgement

This work was supported by BP Chemicals Ltd and EPSRC.

Supplementary material

Crystallographic data and coordinates for theoretical optimised geometries are available in Wiley Interscience. These data can be obtained free of charge via www.ccdc.cam.ac.uk/conts/retrieving.html (or from the CCDC, 12 Union Road, Cambridge CB2 1EZ, UK; fax: +44 1223 336033; e-mail: deposit@ccdc.cam.ac.uk).

REFERENCES

1. Cornils B, Herrmann WA. *Applied Homogeneous Catalysis with Organometallic Compounds (A Comprehensive Handbook in Two Volumes)* V. C. H. Weinheim: New York, 1996.
2. Stille JK, Lau KSY. *Acc. Chem. Res.* 1977; **10**: 434–442; Henderson S, Henderson RA. *Adv. Phys. Org. Chem.* 1987; **23**: 1–62.
3. Maitlis PM, Haynes A, Sunley GJ, Howard MJ. *J. Chem. Soc., Dalton Trans.* 1996; 2187–2196.
4. Haynes A, Maitlis PM, Morris GE, Sunley GJ, Adams H, Badger PW, Bowers CM, Cook DB, Elliott PIP, Ghaffar T, Green H, Griffin TR, Payne M, Pearson JM, Taylor MJ, Vickers PW, Watt RJ. *J. Am. Chem. Soc.* 2004; **126**: 2847–2861.
5. Gelin P, Naccache C, Bentaarit Y. *Pure Appl. Chem.* 1988; **60**: 1315–1320.
6. Chock PB, Halpern J. *J. Am. Chem. Soc.* 1966; **88**: 3511–3514.
7. Haynes A, Mann BE, Gulliver DJ, Morris GE, Maitlis PM. *J. Am. Chem. Soc.* 1991; **113**: 8567–8569; Haynes A, Mann BE, Morris GE, Maitlis PM. *J. Am. Chem. Soc.* 1993; **115**: 4093–4100; Chauby V, Daran J-C, Serra-Le Berre C, Malbosc F, Kalck P, Gonzalez OD, Haslam CE, Haynes A. *Inorg. Chem.* 2002; **41**: 3280–3290; Gonsalvi L, Adams H, Sunley GJ, Ditzel E, Haynes A. *J. Am. Chem. Soc.* 2002; **124**: 13597–13612; Gonsalvi L, Gaunt JA, Adams H, Castro A, Sunley GJ, Haynes A. *Organometallics* 2003; **22**: 1047–1054.
8. Ellis PR, Pearson JM, Haynes A, Adams H, Bailey NA, Maitlis PM. *Organometallics* 1994; **13**: 3215–3226.
9. Griffin TR, Cook DB, Haynes A, Pearson JM, Monti D, Morris GE. *J. Am. Chem. Soc.* 1996; **118**: 3029–3030.
10. Blum J, Weitzberg M, Mureinik RJ. *J. Organomet. Chem.* 1976; **122**: 261–264.
11. Collman JP, Maclaury MR. *J. Am. Chem. Soc.* 1974; **96**: 3019–3020.
12. Huheey JE, Keiter EA, Keiter RL. *Inorganic Chemistry, Principles of Structure and Reactivity* (4th edn). Harper Collins: New York, 1993.
13. Crespo M, Puddephatt RJ. *Organometallics* 1987; **6**: 2548–2550; Puddephatt RJ, Scott JD. *Organometallics* 1985; **4**: 1221–1223.

14. Kinnunen T, Laasonen K. *J. Mol. Struct. (Theochem)* 2001; **542**: 273–288; Ivanova EA, Gisdakis P, Nasluzov VA, Rubailo AI, Rösch N. *Organometallics* 2001; **20**: 1161–1174.
15. Forster D. *Inorg. Chem.* 1972; **11**: 473–475.
16. Forster D. *J. Chem. Soc., Dalton Trans.* 1979; 1639–1645.
17. Yoneda G, Blake DM. *Inorg. Chem.* 1981; **20**: 67–71.
18. Kinnunen T, Laasonen K. *J. Organomet. Chem.* 2001; **628**: 222–232.
19. Bailey NA, Jones CJ, Shaw B, Singleton E. *J. Chem. Soc., Chem. Commun.* 1967; 1051.
20. Pearson JM, Haynes A, Morris GE, Sunley GJ, Maitlis PM. *J. Chem. Soc., Chem. Commun.* 1995; 1045–1046.
21. Perrin DD, Armerego WLF, Perrin DR. *Purification of Laboratory Chemicals* (3rd edn). Pergamon Press: Oxford, 1988.
22. Haynes A, Ellis PR, Byers PK, Maitlis PM. *Chem. Br.* 1992; **28**: 517.
23. Cotton FA, Lahuerta P, Sanau M, Schwotzer W. *Inorg. Chim. Acta* 1986; **120**: 153–157.
24. Forster D. *Inorg. Nucl. Chem. Lett.* 1969; **5**: 433–436.
25. Moser WR. In *Homogeneous Transition Metal Catalysed Reactions*, Moser WR, Slocum DW (eds). *Advances in Chemistry Series*, vol. 230. American Chemical Society: Washington, DC, 1992; 3–18.
26. *SHELXL93*, An integrated system for solving and refining crystal structures from diffraction data: Sheldrick GM, University of Gottingen, Germany, 1993.
27. Frisch MJ, Trucks GW, Schlegel HB, Gill PMW, Johnson BG, Robb MA, Cheeseman JR, Keith T, Petersson GA, Montgomery JA, Raghavachari K, Al-Laham MA, Zakrzewski VG, Ortiz JV, Foresman JB, Cioslowski J, Stefanov BB, Nanayakkara A, Challacombe M, Peng CY, Ayala PY, Chen W, Wong MW, Andres JL, Replogle ES, Gomperts R, Martin RL, Fox DJ, Binkley JS, Defrees DJ, Baker J, Stewart JP, Head-Gordon M, Gonzalez C, Pople JA. *Gaussian 94, Revision D.4*. Gaussian: Pittsburgh PA, 1995.
28. Schlegel HB. *J. Comput. Chem.* 1982; **3**: 214–218.
29. Hay PJ, Wadt WR. *J. Chem. Phys.* 1985; **82**: 270–283; Hay PJ, Wadt WR. *J. Chem. Phys.* 1985; **82**: 299–310.

